Memorias del 2022 Congreso Nacional de Control Automático
12-14 de Octubre, 2022. Tuxtla Gutiérrez, México.

Fundamental aspects of the nonlinear dynamics of a biomass throated tubular gasification reactor

Luis Santamaria-Padilla*, Ulises Badillo-Hernandez*,
Jesus Alvarez ** and Luis Alvarez-Icaza*
** Universidad Nacional Autónoma de México, Instituto de Ingeniería, Ciudad de México, 04510, México*
*** Universidad Autónoma Metropolitana-Iztapalapa, Departamento de Ingeniería de Procesos e Hidráulica, Ciudad de México, 09340, México*

Abstract: As necessary preamble for nonlinear control-estimation design**,** in this study fundamental stationary, transient and robustness characteristics of a spatially distributed tubular throated gasification tristable reactor are studied with efficient PDE-to-ODE discretization. The reactor is described by 15 nonlinear PDEs and has 5 steady-states (SSs): (i) 3 stable ones (nominal with high conversion, grate with intermediate conversion and extinction with null conversion) and (ii) 2 unstable ones (with high [H] and low [L] conversion). On the basis of process insight and extensive numerical simulation, perturbed initial conditions close to the hypersurface separatrix that divides the basins of attraction of the nominal (of interest) and recently reported grate (with less energetic yield) stable SSs were identified, verifying: the existence of the hypersurface separatrices that divide the basins of attraction of the stable nominal-H unstable saddle and L unstable saddle-stable extinction SS pairs. The comparison of the shapes and caloric efficiency of the nominal, grate stable as well as high-conversion unstable SS profiles yielded that: (i) the nominal stable SS exhibits the smallest production of undesirable tar, followed by the H unstable SS and the grate stable SS, and (ii) the temperature and biomass concentration profiles of the high-yield unstable SS and the grate stable SS are rather similar, and appreciable different from the nominal stable SS. With transients induced by pos/negative initial profile temperature deviations it was found: (i) which stable SSs is reached, and (ii) what the settling time, damping and profile front displacement are.

Keywords: throated gasifier, exothermic tubular reactor, distributed system, nonlinear dynamics, PDE numerical method, multiplicity, bifurcation, robustness, transient behavior, energetic yield.

1. INTRODUCTION

Gasification is the conversion of carbonaceous solid fuels into gaseous products (called syngas) with usable heating value (Basu, 2018), and is an attractive technology to assist in environmental problems posed by the disposal of wastes (McKendry, 2002).

The process is carried out into tubular reactors (called gasifiers), being the downdraft type (solid and gas streams flows in the same direction) the more suitable for small-scale applications (10 kW − 10 MW), for which exists the stratified and throated (also called Imbert) configurations, being the later the most installed at gasification systems (Susastriawan et al., 2017). The differences between the two configurations are:

- Internal geometry. Uniform for the stratified and with a V-shape (throat) for the Imbert one.
- Location of the feed inputs. For the stratified, solids and gases are supplied at the top, while for the Imbert configuration, solids are feed at the top, and gases at the throated section.

On reviews of the state-of-art of gasifiers modeling (Patra and Sheth, 2015), are reported the techniques that have been employed, here suffices to state that when partial differential equations (PDE) are employed, the resulting computational models involve the numerical solution of 460 to 53,155 simultaneous ordinary differential equations (ODE), this number can vary depending on the number of PDE considered, as well as the discretization scheme selected by the numerical solver. It is worth mention that the studies have been restricted to the operation at (or around) an ignition steady state.

From modeling studies in tubular reactor engineering (Baldea and Daoutidis, 2012), it is known that nonlinear phenomena, such as multiplicity of steady states (SS), limit cycles, and bifurcation due to changes on inputs or parameters, have a strong influence on the dynamic behavior of the system (Varma, 1980). For reactors with many profiles (Amundson and Arri, 1978; Zitlalpopoca-Soriano et al., 2010), the assessment of the nonlinear dynamics has been limited because the computational load of the numerical continuation-

based packages (Kuznetsov, 1996), commonly employed to determine the multiplicity of SSs,
grows rapidly with the number of equations, their ill conditioning, and their multiplicity patterns (Allgower and Georg, 1990). The novel efficient modeling scheme for tubular heterogeneous reactors proposed by Badillo-Hernandez et al. (2019), gives a criterion to determine the PDE-to-ODE discretization order of a model that provides a reliable-quantitative description (preserving the SSs and the nonlinear dynamic behavior), it has been applied for a 12-profile stratified gasifier and for a 15-profile throated gasifier, determining that at nominal feed conditions the gasifiers exhibit bistability and tristability, respectively.

In our previous study (Santamaria-Padilla et al., 2022), an Imbert gasifier was modeled and studied, finding that at nominal operation conditions it has 5 steady states (SS), being:

- 3 stables: nominal, grate, and extinction, with high, intermediate and null conversion, respectively.
- 2 unstable ignition-type of: high (H) and low (L) conversion.

The grate SS: (i) has incidentally appeared in simulation-based studies of the effect of input in the stable SS of interest, (Simone et al., 2013), (ii) lacks formal characterization in the light of multiplicity, and (iii) requires adequate validation with transient simulation designed for the purpose at hand. These considerations motivate the main aim of the present study: the verification of the existence of the hypersurface separatrices that divide the basins of attraction of the stable nominal-H unstable saddle and L unstable saddle-stable extinction SS pairs. Additionally, in this work aspects not considered in previous studies (Santamaria-Padilla et al., 2022) are addressed: (i) a comparison between the profile shape and caloric efficiency of the nominal, grate stable SSs as well as high conversion unstable SS is performed, and (ii) basic transient response characteristics (settling time, overshoots, and profile front displacement) due to trajectories induced by deviations around the temperature profiles of the unstable SSs are studied.

The results of the present study complete the single-SS stable stationary (the one of interest) (Santamaria-Padilla et al., 2016) and multiplicity (the nominal one plus 2 or 4 SSs) (Santamaria-Padilla et al., 2022) ones of our previous studies on the same subjects, as a fundamental and necessary step for nonlinear estimation and control designs in future studies.

In section 2, the throated gasifier is described, then the general form of the PDE model as well as its differential algebraic equation (DAE) form is presented, accompanied with the efficient order and the nominal feed conditions employed. In section 3, the temperature and biomass concentration profiles are shown, as well as the syngas composition for all the SSs, to be aware of the performance differences between them; then the trajectories that start on the neighborhood of the unstable SSs are shown to discuss basic aspects of the transient response, as well as to verify the existence of the separatrices that divide the basins of attraction. Finally, on section 4, the conclusions withdrawn from this work are presented.

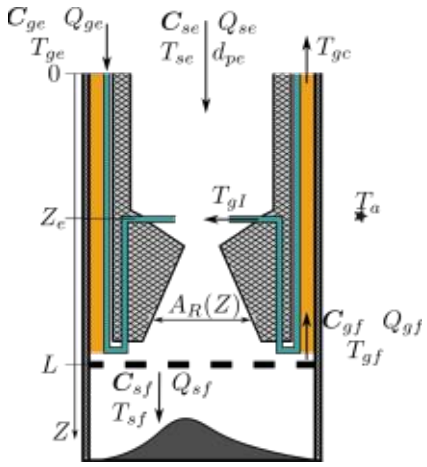

Fig. 1. Imbert gasifier with air preheating, adapted from Santamaria-Padilla et al. (2022)

2. IMBERT GASIFIER MODEL

Consider the Imbert gasifier of length L depicted on Fig. 1, where solid biomass (with volumetric flow Q_{se}, particle size d_{pe}, concentration $\boldsymbol{C}_{se}$, and temperature T_{se}) and cold air feed streams (with volumetric flow Q_{ge}, concentration $\boldsymbol{C}_{ge}$, and temperature T_{ge}), are converted into syngas (with volumetric flow Q_{gf}, concentration $\boldsymbol{C}_{gf}$, and temperature T_{gf}) and char (with volumetric flow Q_{sf}, concentration $\boldsymbol{C}_{sf}$, and temperature T_{sf}) through a multicomponent-multireaction (pyrolysis, combustion, reduction, cracking, reforming, and water gas-shift) exothermic network (Di Blasi, 2000). The incoming cold air is preheated with the hot syngas stream, and it is injected at the throated section of the reactor, which enhances the mass-transport and reaction rate, and increases the overall energetic efficiency of the process (Susastriawan et al., 2017).

2.1 General model

The gasifier with air preheating has been modeled with due closure on Santamaria-Padilla et al. (2022), by considering standard modeling assumptions such as: (i) thermal equilibrium between solid-gas phases, (ii) quasi steady state for gas phase, and (iii) nonreactive flow on the heat exchanger. The above yielded the following ordinary partial differential equation (OPDE) model in general form

$$\partial_t \boldsymbol{\chi} = \boldsymbol{F}_{\chi}(\boldsymbol{\chi}, \boldsymbol{\psi}, \partial_Z \boldsymbol{\chi}, \partial_{ZZ} \boldsymbol{\chi}, \boldsymbol{d}, \boldsymbol{p}) \quad (1a)$$

$$\boldsymbol{0} = \boldsymbol{F}_{\psi}(\boldsymbol{\chi}, \boldsymbol{\psi}, \partial_Z \boldsymbol{\psi}, \boldsymbol{d}, \boldsymbol{p}), \qquad 0 \le Z \le L, \quad t \ge 0 \quad (1b)$$

with boundary and initial conditions

$$\boldsymbol{B}_{\chi}(\boldsymbol{\chi}, \boldsymbol{\psi}, \partial_Z, \boldsymbol{d}, \boldsymbol{p}) = \boldsymbol{0}; \ \boldsymbol{B}_{\psi}(\boldsymbol{\chi}, \boldsymbol{\psi}, \boldsymbol{d}, \boldsymbol{p}) = \boldsymbol{0}; \ \boldsymbol{\chi}(\boldsymbol{0}) = \boldsymbol{\chi}_{\boldsymbol{0}}$$

where

$$\boldsymbol{\chi}(t) = [\boldsymbol{C}_s\ T\ T_h]^T(Z,t) \quad (1c)$$

$$\boldsymbol{\psi}(t) = \left[Q_g\ Q_s\ \boldsymbol{C}_g^T\ T_c\right]^T(Z,t) \quad (1d)$$

$$\boldsymbol{d} = \left[Q_{se}\ Q_{ge}\ \boldsymbol{C}_{se}^T\ \boldsymbol{C}_{ge}^T\ T_{se}\ T_{ge}\ T_a\right]^T \quad (1e)$$

$\boldsymbol{\chi}$ (or $\boldsymbol{\psi}$) is the set of dynamic (or quasi static) profiles, $\boldsymbol{F}_{\boldsymbol{\chi}}$ (or $\boldsymbol{F}_{\boldsymbol{\psi}}$) is a differential spatial domain operator with boundary condition $\boldsymbol{B}_{\boldsymbol{\chi}}$ (or $\boldsymbol{B}_{\boldsymbol{\psi}}$), $\partial_Z\boldsymbol{\chi}$ (or $\partial_{ZZ}\boldsymbol{\chi}$) is the first (or second) partial derivative with respect to the spatial domain, ∂_t is the first partial derivative with respect to the temporal domain, $\boldsymbol{\chi_0}$ is a vector with the initial conditions of the dynamic profiles, $\boldsymbol{d}$ is a vector with the exogenous inputs, $\boldsymbol{p}$ is a vector with the kinetic-transport (KT) parameters, $\boldsymbol{C}_s$ is a vector with the solid profiles (biomass, moisture and char), $\boldsymbol{C}_g$ is a vector with the gas profiles (O_2, CO, CO_2, H_2, CH_4, H_2O, Tar), T is the temperature of the solid-gas bed inside the reactor, T_h (or T_c) is the temperature of the syngas (or the incoming air) at the annular section (or the pipes), Q_s (or Q_g) is the solid (or gas) volumetric flow, and T_a is the surrounding temperature.

The application of spatial finite difference discretization (Hundsdorfer and Verwer, 2003) to the OPDE model (1), yields the N-order differential algebraic equation (DAE)

$$\dot{\boldsymbol{x}} = \boldsymbol{f}_{\boldsymbol{x}}(\boldsymbol{x},\boldsymbol{\zeta},\boldsymbol{d},\boldsymbol{p},N), \boldsymbol{x}(0) = \boldsymbol{x}_0 \quad (2a)$$

$$\boldsymbol{0} = \boldsymbol{f}_{\boldsymbol{\zeta}}(\boldsymbol{x},\boldsymbol{\zeta},\boldsymbol{d},\boldsymbol{p},N), N \in \mathcal{N} \quad (2b)$$

$$n = n_{\boldsymbol{x}} + n_{\boldsymbol{\zeta}} \quad (2c)$$

where

$$n_{\boldsymbol{x}} = \dim \boldsymbol{x} = (n_s + 2)N, n_{\boldsymbol{\zeta}} = \dim \boldsymbol{\zeta} = \big(n_g + 3\big)N$$

$\boldsymbol{x}$ (or $\boldsymbol{\zeta}$) is the dynamic (or quasi static) state variable, $n_{\boldsymbol{x}}$ (or $n_{\boldsymbol{\zeta}}$) is the number of differential (or algebraic) equations, n is the total number of differential and algebraic equations, n_s (or n_g) is the number of solid (or gas) species, and N is the model order.

2.2 Efficient model order

The efficient modeling approach (Badillo-Hernandez et al., 2019), provides a method to the determine the smallest integer order $N = N_S$ (smaller than the N_{pde} employed in standard PDE solvers) for which the limit sets (SSs and limit cycles) are preserved in the light of kinetics-transport parameter uncertainty. This approach has been applied to a pilot scale Imbert gasifier (described at subsection 2.3), finding that when it operates at nominal conditions it has 5 SSs (listed at Table 1), without evidence of limit cycles. The above has been determined employing the model (2) with an efficient order

$$N_S = 61 \quad (3)$$

Details on the numerical determination of the efficient model order (3), can be found on Santamaria-Padilla et al. (2022). The related algorithms and computer packages can be found on Badillo-Hernandez et al. (2019) and references there in.

2.3 Case study

The gasifier studied in this work is part of a pilot scale gasification system (AllPowerLabs, 2021) that can produce up to 10 kW, has length $L =$ 0.55 m, operates with wood chips, is instrumented with 7 type-K thermocouples along the reactor and a gas analyzer at the exit of the heat exchanger, and has the nominal feed conditions of Table 2. Further details on the parameters, experimental data, and particular characteristics of the system can be found on Yucel and Hastaoglu (2016).

Table 1. Steady states of the Imbert gasifier

Name (stability)	Nomenclature	Energetic yield
Extinction (stable)	$\overline{\boldsymbol{x}}_E$	Null
Low conversion (unstable)	$\overline{\boldsymbol{x}}_L^u$	Low
Grate (stable)	$\overline{\boldsymbol{x}}_G$	Intermediate
High conversion (unstable)	$\overline{\boldsymbol{x}}_H^u$	High
Nominal (stable)	$\overline{\boldsymbol{x}}_I$	Highest

Table 2. Nominal feed conditions

Property	Value
Solid flow (kg/hr)	3.8
Air to biomass ratio	1.2
Solid moisture (%)	7.28

3. ANALYSIS OF THE STEADY STATES

The numerical simulations performed in this section consider the model (2), with the efficient order $N_S = 61$ (3). The corresponding hypersurface separatrix between the state ignition-grate SS pair is so that a 915-dimensional.

3.1 Steady state profiles comparison

On Fig. 2 are shown the temperature (T) and biomass concentration (ρ_B) profiles at SS, on continuous line are plotted the stable SSs and on discontinuous line the unstable ones.

From the T-profile (top of Fig. 2) can be seen that: (i) the nominal SS $\overline{T}_I$ describes adequately the experimental data reported by Yucel and Hastaoglu (2016), and (ii) the grate SS $\overline{T}_G$ does not describe the data of the first 6 thermocouples (from the top to the bottom), but at the last measurement there is a difference of about 40 K. The high unstable SS profile $\overline{T}_H$ is very similar to the grate one $\overline{T}_G$, the main differences are at the first 0.4 m, being below (or above) the temperature profile from 0-0.25 m (or 0.25-0.4 m), while the hotspot of the $\overline{T}_H$ profile is located 0.03 m above the one of the $\overline{T}_G$ one with a temperature difference of 28 K. For the low unstable SS $\overline{T}_L$, the maximum temperature that can attain is at the bottom of the reactor and does not describe any of the temperature measurements. Finally, the extinction SS $\overline{T}_E$ is at ambient temperature (300 K) since there is no reaction inside the gasifier.

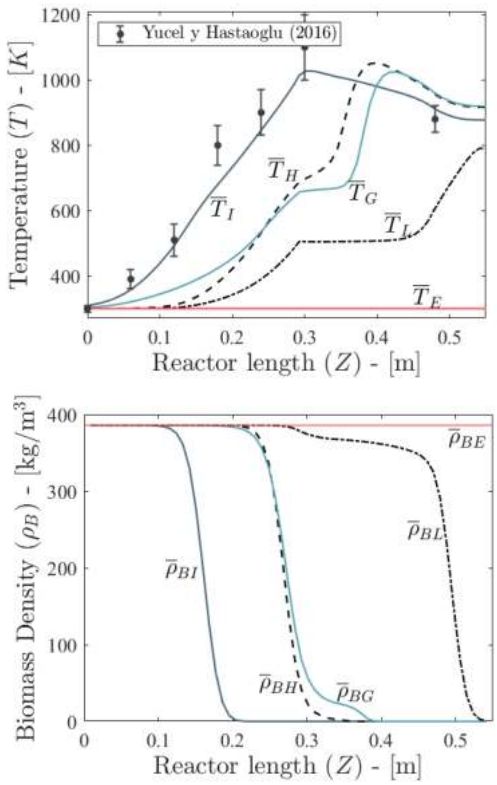

Fig. 2. Temperature and biomass density profiles at SS

The ρ_B-profile (bottom of Fig. 2) provides the information about the locations at which the chemical reactions begin. For the $\overline{\rho}_{BI}$ SS profile can be seen that it begins to decrease at 0.1 m, which implies that the pyrolysis starts at that point, for the $\overline{\rho}_{BH}$ and $\overline{\rho}_{BG}$ SS profiles the pyrolysis begins at about 0.23 m, while for the $\overline{\rho}_{BL}$ SS it slowly takes place at around 0.28 m with major changes at 0.48 m. The gaseous products are determined by the way in which the pyrolysis occurs.

3.2 Syngas comparison at SS

On Table 3 (recovered from Santamaria-Padilla et al., 2022), are reported the molar fractions and the lower heating value (LHV) of the syngas, as well as the cold gas efficiency (CGE). Focusing on the LHV and the CGE, it can be seen that the nominal, grate and high unstable SSs have very similar values, the above implies that they are suitable to operate and satisfy energetic demands that are between 4 to 6 MJ/Nm^3 (Pérez et al., 2012; Simone et al., 2013; Yucel and Hastaoglu, 2016).

Table 3. Syngas composition and performance indexes

SS	Molar fraction [%]					LHV	CGE
	H_2	CO	CO_2	CH_4	Tar	[MJ/m^3]	[%]
Nominal	15.5	21.5	10.2	2.97	0.3	5.417	62.5
High	13.6	21.6	8.7	2.6	1.9	5.118	61.6
Grate	12.0	18.3	9.8	2.7	2.5	4.584	51.4
Low	4.6	4.5	4.8	1.0	13.9	1.429	15.8
Extinction	0	0	0	0	0	0	0

Focusing on the amount of tars that are produced at each SS, with respect to the value at the nominal SS there is an increase of 5.5 (or 7.4) times on the tar content of the high unstable (or grate stable) SS, which implies that the syngas must be carefully cleaned up (at a subsequent stage) to prevent damage on other components of the gasification system, especially in the case where the syngas effluent is used as fuel of an internal combustion engine. Finally, the low SS is not adequate to operate since it has poor LHV and CGE values.

3.3 Characteristics of the transient behaviour

On the basis of process insight and extensive numerical simulation trials, perturbed initial conditions close to the hypersurface separatrix that divides the basins of attraction of the nominal (of interest) and recently reported grate (with less energetic yield) stable SSs were identified, verifying the existence of such separatrix induced by the presence of the grate SS. In the same way, perturbed initial conditions close to the hypersurface separatrix that divides the basins of attraction of the grate (with less energetic yield) and extinction (with null energetic yield) stable SSs were identified, verifying the existence of such separatrix induced by the presence of the grate SS.
The disturbances on the initial conditions must be carefully chosen, so that the mass and energy balances of the system remain satisfied. After several trials, was found that it is convenient to disturb only the temperature profile, which corresponds to a vector with 61 elements in the 915-dimension hypersurface that determines the behavior of the gasifier. For other disturbances on the initial conditions, e.g. on the solid profile, the numerical solver underwent divergence difficulties underlain by since the mass balance inconsistencies.

Consider the trajectories

$$\boldsymbol{x}_i(t) = \boldsymbol{\tau}_{\boldsymbol{x}}\left(t, \boldsymbol{x}_0^i, \overline{\boldsymbol{d}}, N\right),\ i = 1, \ldots, 4,\quad N = N_S \qquad (4)$$

that are generated due to the nominal input $\overline{\boldsymbol{d}}$, with initial conditions of the dynamic states $\boldsymbol{x}_0^i$ equal to the high ($\overline{\boldsymbol{x}}_H^u$) and low ($\overline{\boldsymbol{x}}_L^u$) SSs with a disturbance on the temperature profile

$$\boldsymbol{x}_0^i = \left[\overline{\boldsymbol{C}}_{s,H}^T\ w_i\overline{T}_H\ \overline{T}_{h,H}\right]^T,\ i = 1,2$$

$$\boldsymbol{x}_0^i = \left[\overline{\boldsymbol{C}}_{s,L}^T\ w_i\overline{T}_L\ \overline{T}_{h,L}\right]^T,\quad i = 3,4$$

where

$$\boldsymbol{w} = [w_1\ w_2\ w_3\ w_4]^T = [1.02\ \ 0.98\ \ 1.02\ \ 0.98]^T$$

is a vector with the corresponding weights to disturb the temperature profile of the unstable SSs by $\pm 2\%$, these disturbances are adequate to verify the existence of the separatrices that divide the basins of attraction of the stable SSs.

In Figs. 3 and 4 the temperature profile evolutions of trajectories (4) are shown, and behave as follows: (i) $\boldsymbol{x}_1(t)$ ends up at the nominal SS (top of Fig. 3) with a settling time

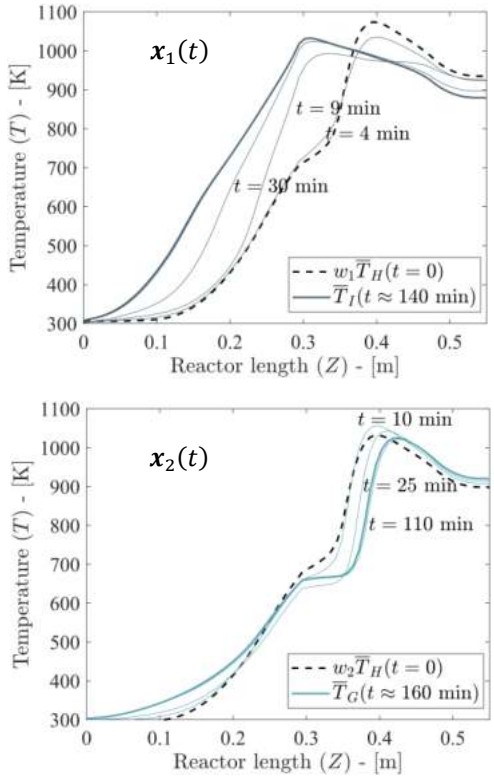

Fig. 3. Temperature profile evolutions starting on the neighborhood of the high unstable SS

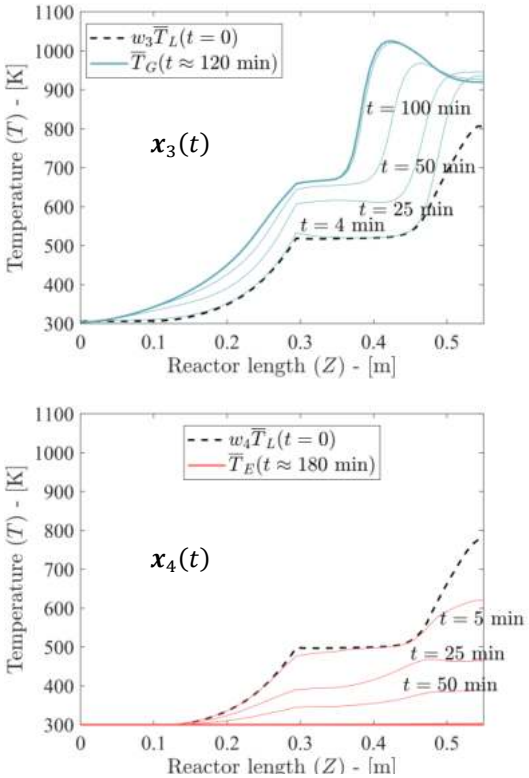

Fig. 4. Temperature profile evolutions starting on the neighborhood of the low unstable SS

of 140 min and without overshoots, and hotspot displaced 0.02 m to the top, (ii) $\boldsymbol{x}_2(t)$ exhibits small downshoots (that ranges from 5 to 2%) before it attains the grate SS (bottom of Fig. 3) with a settling time of 160 min, and exhibits hotspot displacement of 0.03 m to the bottom, (iii) $\boldsymbol{x}_3(t)$ goes towards the grate SS (top of Fig. 4) with small overshoots (of 4% maximum) on the last 0.05 m, with a settling time of 120 min, and 0.11 m hotspot displacement towards the top, and (iv) $\boldsymbol{x}_4(t)$ reaches the extinction SS (bottom of Fig. 4) with a settling time of 180 min.

The trajectories $\boldsymbol{x}_1(t)$ and $\boldsymbol{x}_2(t)$: (i) start in the neighborhood of the $\overline{\boldsymbol{x}}_H^u$ SS temperature profile, but (ii) converge towards the SSs $\overline{\boldsymbol{x}}_I$ and the $\overline{\boldsymbol{x}}_G$, respectively, both being faster (by 20 min) $\boldsymbol{x}_1(t)$. For the trajectories $\boldsymbol{x}_3(t)$ and $\boldsymbol{x}_4(t)$, they start in the neighborhood of the $\overline{\boldsymbol{x}}_L^u$ SS temperature profile, reaching the SSs $\overline{\boldsymbol{x}}_G$ and $\overline{\boldsymbol{x}}_E$, respectively, with a 60 min settling time difference. The trajectories $\boldsymbol{x}_2(t)$ and $\boldsymbol{x}_4(t)$, that require more sensible energy dissipation, are the slower ones, with settling times of 160 and 180 mins, respectively. The trajectories $\boldsymbol{x}_1(t)$ and $\boldsymbol{x}_3(t)$, that require increase of sensible energy on the process, are the fastest ones, with settling times of 140 and 120 mins, respectively.

The preceding results verify the existence of the separatrices that divide the basins of attraction of the stable nominal-H unstable saddle and L unstable saddle-stable extinction SS pairs.

4. CONCLUSIONS

Fundamental stationary, transient and robustness characteristics of a tubular throated gasification tristable reactor have been characterized with efficient nonlinear PDE modeling. Due to process insight and from several numerical simulations performed, perturbed initial conditions close to the hypersurface separatrix that divides the basins of attraction of the nominal (of interest) and grate (with less energetic yield) stable SSs were identified, which verify the existence of the separatrices.

With steady state analysis, it was found that the nominal stable SS yields the smallest tar production, followed by the high-yield unstable and the grate stable SSs, and the temperature biomass concentration profiles of the high-yield unstable SS and the grate stable SS are rather similar, and appreciable different from the nominal stable SS. With transient simulations due to initial profile temperature disturbances, the corresponding stable SSs attained were found, also the transient characteristics of settling time, damping and profile front displacement were determined for each trajectory.

The results of this study complete the stationary analysis of the nominal SS (the one of interest) (Santamaria-Padilla et al., 2016) and multiplicity (the nominal one plus 2 or 4 SSs) (Santamaria-Padilla et al., 2022) ones of our previous works on the same subjects, as a fundamental and necessary step for nonlinear estimation and control designs in future studies, which must be focused in the enhancement of robustness of the nominal operation and in attaining a basin of attraction as large as possible, with adequate disturbance rejection capability and temperature regulation at the measurement location. Also, this study is the departure point to analyze in detail the transient response due to exogenous disturbances on the air feed flow, as well as the startup of the gasifier, with awareness on the multiplicity pattern that the gasifier possess. The results are a key point of departure to address in a tractable manner the efficient model-based nonlinear feedback control and estimation problems.

REFERENCES

Allgower, E. L., & Georg, K. (1990). Numerical continuation methods. An introduction. *Springer Series in Computational Mathematics*, 388.

AllPowerLabs. (2021). All power labs. Retrieved June 5, 2021, from http://www.allpowerlabs.com/

Amundson, N. R., & Arri, L. E. (1978). Char gasification in a countercurrent reactor. *AIChE Journal*, *24*(1), 87–101. https://doi.org/10.1002/aic.690240110

Badillo-Hernandez, U., Alvarez, J., & Alvarez-Icaza, L. (2019). Efficient modeling of the nonlinear dynamics of tubular heterogeneous reactors. *Computers and Chemical Engineering*, *123*, 389–406. https://doi.org/10.1016/j.compchemeng.2019.01.018

Baldea, M., & Daoutidis, P. (2012). Dynamics and nonlinear control of integrated process systems. In *Dynamics and Nonlinear Control of Integrated Process Systems* (Vol. 9780521191). https://doi.org/10.1017/CBO9780511978760

Basu, P. (2018). Biomass gasification, pyrolysis and torrefaction: Practical design and theory. In *Biomass Gasification, Pyrolysis and Torrefaction: Practical Design and Theory*. https://doi.org/10.1016/C2016-0-04056-1

Bindel, D., Jonkhout, C., Govaerts, W., Hughes, J., Kuznetsov, Y. A., Pekker, M., & Veldman, D. (2019). *CL_MATCONTL2019: continuation toolbox in MATLAB*. Retrieved from http://uah.edu/faculty/pekker

Di Blasi, C. (2000). Dynamic behaviour of stratified downdraft gasifiers. *Chemical Engineering Science*, *55*(15), 2931–2944. https://doi.org/10.1016/S0009-2509(99)00562-X

Hundsdorfer, W., & Verwer, J. G. (2003). Numerical Solution of Time-Dependent Advection-Diffusion-Reaction Equations. In *SIAM Review* (Vol. 33).

Kuznetsov, Y. A. (1998). Elements of Applied Bifurcation Theory. In *Elements of Applied Bifurcation Theory*. https://doi.org/10.1007/b98848

McKendry, P. (2002). Energy production from biomass (part 3): Gasification technologies. *Bioresource Technology*, *83*(1), 55–63. https://doi.org/10.1016/S0960-8524(01)00120-1

Patra, T. K., & Sheth, P. N. (2015, October 1). Biomass gasification models for downdraft gasifier: A state-of-the-art review. *Renewable and Sustainable Energy Reviews*, Vol. 50, pp. 583–593. https://doi.org/10.1016/j.rser.2015.05.012

Pérez, J. F., Melgar, A., & Benjumea, P. N. (2012). Effect of operating and design parameters on the gasification/combustion process of waste biomass in fixed bed downdraft reactors: An experimental study. Fuel, 96, 487–496. https://doi.org/10.1016/j.fuel.2012.01.064

Santamaria-Padilla, L., Alvarez-Icaza, L., & Alvarez, J. (2016). "Modelado con validación experimental de un gasificador de biomasa." *Memorias del Congreso Nacional de Control Automático, Querétaro, Querétaro, México*. 2016.

Santamaria-Padilla, L., Badillo-Hernandez, U., Álvarez, J., & Álvarez-Icaza, L. (2022). On the nonlinear dynamics of biomass throated tubular gasification reactors. *Computers & Chemical Engineering*, 107828. https://doi.org/10.1016/j.compchemeng.2022.107828

Simone, M., Nicolella, C., & Tognotti, L. (2013). Numerical and experimental investigation of downdraft gasification of woody residues. *Bioresource Technology*, *133*, 92–101. https://doi.org/10.1016/j.biortech.2013.01.056

Susastriawan, A. A. P., Saptoadi, H., & Purnomo. (2017). Small-scale downdraft gasifiers for biomass gasification: A review. *Renewable and Sustainable Energy Reviews*, *76*(March), 989–1003. https://doi.org/10.1016/j.rser.2017.03.112

Varma, A. (1980). On the Number and Stability of Steady States of a Sequence of Continuous-Flow Stirred Tank Reactors. *Industrial and Engineering Chemistry Fundamentals*, *19*(3), 316–319. https://doi.org/10.1021/i160075a016

Yucel, O., & Hastaoglu, M. A. (2016). Kinetic modeling and simulation of throated downdraft gasifier. *Fuel Processing Technology*, *144*, 145–154. https://doi.org/10.1016/j.fuproc.2015.12.023

Zitlalpopoca-Soriano, A. G., Vivaldo-Lima, E., & Flores-Tlacuahuac, A. (2010). Bifurcation analysis of a tubular reactor for nitroxide-mediated radical polymerization of styrene. *Macromolecular Reaction Engineering*, *4*(9–10), 599–612. https://doi.org/10.1002/mren.201000003